Observations of large infragravity-wave run-up at Banneg Island, France

Alex Sheremet[1], Tracy Staples[1], Fabrice Ardhuin[2], Serge Suanez[3], and Bernard Fichaut[3]

On Banneg Island, France, very high water-level events (6.5 m above the astronomical tide) have been observed on the western cliff, exposed to large swell from the North Atlantic. The analysis of hydrodynamic measurements collected during the storm of February 10, 2009 shows unusually high (over 2 m) infragravity wave run-up events. A comparison of run-up observations to measurements in approximately 7-m of water, and numerical simulations with a simplified nonlinear model allow two distinct infragravity bands to be identified: an 80-s infragravity wave, produced by nonlinear shoaling of the storm swell, and a 300-s wave, trapped on the intertidal platform of the island and generating intermittent, low-frequency inundation. Our analysis shows that the 300-s waves are a key component of the extreme water levels recorded on the island.

1. Introduction

Infragravity waves (IGW) are ocean waves with characteristic periods of the order of minutes, just above the range of wind-wave periods. They are small in deep water (heights of order of cm; Aucan and Ardhuin, 2013) but play an important role in nearshore processes [e.g., Guza and Thornton, 1982; Guza and Feddersen, 2012]. Most of our knowledge about IGW derives from observations on mild-sloping sandy beaches, where they can develop heights of order of 1 m, [e.g., Guza and Thornton, 1982; Kaihatu and Kirby, 1995; Sheremet et al., 2002, and many others]. It is widely agreed that they are generated by nonlinear mechanisms in shallow water and have important consequences for shoreline erosion, coastal inundation, and coastal hazards. For example, the IGW regime can change locally the position of the water table and alter erosion and accretion processes in the swash zone, and might be related to periodic beach morphology [e.g., Coco et al., 2004; Huisman et al., 2011, and others]. The relation between IGW run-up and offshore wave conditions [Senechal et al., 2011; Guza and Feddersen, 2012], and the dynamics of the saturated run-up spectrum [e.g., Bryan and Coco, 2010] are still not well understood.

On steep, rocky shorelines the dynamics of water-levels and IGW change: waves shoal rapidly, develop large frontal accelerations, and produce a narrow, highly localized surf zone with plunging breakers and large dissipation rates [Sheremet et al., 2011]. Wave-generated currents are intermittent, with strong shoreward jets followed by slow seaward back-flows. Wave setup and IGW modulate both breaking location and current patterns. Seiching and anomalous inundation patterns have been observed [Vetter et al., 2010; Nwogu and Demirbilek, 2010]. In situ measurements on steep bathymetry and under plunging breakers are difficult, even in low energy conditions – which makes such observations both rare and valuable.

Extreme storm damage is often found at very high elevations above the mean water level, with occasional quarrying of blocks from the cliff top and their deposition inland, in the form of "cliff-top storm deposits" [Hansom et al., 2008; Fichaut and Suanez, 2011]. These deposits have been attributed to the direct attack of very large waves on the cliff face. Such remarkable deposits of huge boulders, some of which were apparently transported across the island (see supporting auxiliary material), were repeatedly recorded on the small French island of Banneg (Figure 1). The most recent event occurred during the March 10, 2008 storm, at the time of a spring tide [Cariolet et al., 2010; Fichaut and Suanez, 2011], suggesting that combined high water levels and large IGW run-up are essential for quarrying, transport, and deposition of blocks on Banneg Island. Here we show (Section 2) that the recorded run-up on Banneg is dominated by low-frequency nearshore IGWs of unexpected high amplitudes. In Section 3 we use a simple nonlinear model in section 3 to try and explain this IGW generation, and discuss possible explanations for the generation of the large IGW observed.

2. Observations and data analysis

Banneg is an 800 m long, 150-m to 350-m wide island in the Molène Archipelago (Figure 1a) off the north-western coast of Brittany, France. On the west side the submerged slope is 0.04 on average, with the 50-m isobath approximately 1,200 m offshore (Figure 1a-b). The island is partially sheltered from the large Atlantic swells by its larger neighbor island of Ouessant, typically resulting in wave heights 40% smaller compared to the open ocean [Ardhuin et al., 2011]. Wave propagation between Ouessant and Banneg is affected by strong currents, especially in the Fromveur passage between the two islands where the currents can exceed 3 m/s during neap tides. Such currents can block waves of 7.6 s, and focus and steepen 12-s swells. Such swells typically propagate out of the West [Ardhuin et al., 2012], often at a wide angle with respect to the exposed island shoreline (e.g., Figure 1a). A remarkable feature of the island is the presence of an intertidal platform of significant width (Figure 1a), surrounding a supratidal platform bordered by cliffs with slopes between 1.0 and 3.0 (on the western side). The supratidal platform has a mean elevation of 5 m above the maximum tide, and 10 m above mean sea level [Fichaut and Suanez, 2011].

Field observations conducted in winter 2008-2009 included six pressure sensors deployed on the western side of the island. This study focuses on measurements collected at three sensors (P2, P3, and P4 Figure 1a,c). Sensors P3 and P2 were located approximately on a cross-shore transect at 1.30 and 7.52 m above the chart datum (Figure 1b), namely 4.7 m below and 1.52 m above the mean sea level. Sensor P4 was located approximately 150 m south of the P3-P2 transect, close to the chart datum. Ardhuin et al. [2011] estimates that at sensor P3 the 30-minute mean water level reaches 60 cm above the astronomical tide, giving a 30-minute average level of 7.3 m. At P2, the mean water level is ill-defined due to dry-out

[1]Department of Civil and Coastal Engineering, University of Florida, Gainesville, Florida, USA.

[2]IFREMER, Laboratoire d'Océanographie Spatiale, Plouzané, France.

[3]LEGT-Géomer-Brest, IUEM, Plouzané, France.

Figure 1. a) Banneg Island bathymetry, with the outline of the island (red). Outer line: contour of the inter-tidal platform; Inner line: the supra-tidal platform of the island. The approximate location of the sensors P2, P3, and P4 on the intertidal platform marked with a red circle (sensors not resolved at this scale). The typical propagation direction of storm waves (toward NNE, approximately 60 degrees counterclockwise from East.) Inset: Bretagne, the Molène Archipelago, and Banneg Island. b) Large-scale cross-section of Banneg Island bathymetry along the dashed line in panel a). c) Approximate cross-section of the bathymetry at the location of the sensors. d) A photograph of the location of P2.

Figure 2. Free surface elevation recorded on Feb. 10th, 2009 04:00 - 04:10 UTC at a) P2 and P3. b) Detail of time series (segment marked by a black box on panel a). The vertical reference in all panels is the chart datum. Dasher line in Panel b represents the location of the P2 sensor.

periods that amount to roughly 10% of the time. During the wet times, the mean depth is 2.5 m, which corresponds to a water level 1.7 m above the mean water level at P2.

The goal of this study is to investigate the large, slow water-level oscillations recorded at P2 (Figure 2a), during a storm that occurred at a spring high-tide, on Feb. 10, 2009, around 4:00 hours UTC. The significant wave height between the islands of Ouessant and Banneg was estimated at 5 m, with a peak period of 13 s. The origin of these large oscillations (sometimes exceeding 2.5 m in height) is not obvious. Their periodicity (order of minutes) is consistent with infragravity waves; the shape of the signal, a steep front followed by a gradual decrease in elevation, is similar to lab-

oratory IGW run-up measurements (e.g., Figure 8 in Nwogu and Demirbilek, 2010, run-up gauge, 34.5 s group period).

However, visual inspection does not detect any obvious relation between the P2 and P3 time series (Figures 2a and 2b) – as one would expect, given the small distance between the sensors. Moreover, the interpretation of the infragravity P2 time series (e.g., Figure 2a,c) is complicated by the fact that the sensor could have been submerged only part of the time. Indeed, wave-troughs appear to be cut off during lower water levels (Figure 2c). Due to alternating wet/dry periods of the sensor, the analysis of the P2 observations is expected to be biased to an unknown degree.

Both standard Fourier analysis and time-frequency (wavelet) decomposition techniques were used to interpret the data. Time-frequency (wavelet) techniques could in principle avoid the distortions produced by time-series truncation. However, during the analysis, it soon became clear that the Fourier results were robust and produced consistent results. We therefore base this discussion only on the Fourier analysis results. Data was analyzed using spectral and cross-spectral Fourier techniques. The 150-min (45000 points sampled at 5 Hz) time series was de-meaned, detrended, and divided into 50% overlapping segments of 4096 points (approximately 13.4 min), resulting in spectral estimates with 20 DOF (degrees of freedom). Smooth bispectral estimates [Elgar et al., 1995] were calculated with 80 DOF.

In addition to data analysis, preliminary numerical simulations were conducted using a unidirectional version of a phase-resolving, nonlinear mild-slope model developed by Agnon and Sheremet [1997]; Sheremet et al. [2011]. The model describes the cross-shore evolution of Fourier modes of the free-surface displacement due to nonlinear (3-wave) interactions and various dissipation/growth mechanisms (e.g. wind input, white capping, bottom friction, etc). In the runs presented here, the only dissipation included was the frequency-distributed, depth-limited breaking [Thornton and Guza, 1983; Kaihatu and Kirby, 1995]. The model was run for a bathymetry transect corresponding to the oblique incidence angle (Figure 1a), complemented with a high-resolution shallow water transect (Figure 1b). The model was initialized in 50-m of water with a JONSWAP spectrum (13-s peak period; 5-m significant height), corresponding roughly to the conditions expected during the Feb. 10th, 2009 storm. However, because this does not provide information about the IG waves, the second-order bound IGW spectrum associated with the deep water swell was computed using a Stokes-type expansion of the nonlinear mild slope equation [Agnon et al., 1993].

Figure 3. Spectral and cross-spectral analysis of P2 and P3 measurements (P4 records are similar to P3). Left: full spectrum. Right: infragravity band. a,d) Estimates of spectral density of variance at P2 (red), P3 (blue). b,e) Cross-spectral phase (phase lag between P2 and P3); c,f) Coherency. Panel e), red circles: progressive-wave content R, equation 3. Shaded boxes in d) e) and f) mark the 300-s and 80-s bands.

3. Results and discussion

The basic assumption that the P2 time series is truncated (trough cut-off) to an unknown degree (as suggested in Figure 2c) implies the existence of a "true" signal that was incompletely observed. The "true" signal could be defined as the run-up. For the steep Banneg slopes, and at the very low IG frequencies, this is analogous with the sensor being mounted on a vertical boundary just above the troughs. This type of observations (overland measurements) are quite common in tsunami studies [e.g., Fritz et al., 2006]. Any conjectures made about the "true" signal based on the truncated observations are expected to be biased, to an unknown degree.

Even though the degree of bias is unknown, based on tested on synthetic data, we expect the truncated signal to exhibit a number of distortions by comparison to the "true" signal: a lower variance than the "true" signal; a larger variance at high frequencies; a lower coherency, possibly more severe at low frequencies, as they have less statistical stability; and a larger sum-interaction coupling (e.g.,

the bispectral phase correlation between the peak and its harmonics).

Fortunately, an examination of the analysis results shows enough consistency and stability to conclude that the effects of truncation are small. The estimated variance density spectra at P2 and P3 (Figure 3a,d) are consistent. The slower decay with frequency of the P2 high-frequency band might be due to dynamic pressure induced by waves colliding with the cliff. The spectral peak is lower at P2, as one would expect from wave breaking. Cross-spectral results for P2 and P3 (Figure 3b,c,e,f; P2-P4 analysis yields similar results) are consistent and stable for $10 \leq DOF \leq 40$. The coherency between P2 and P3 (Figure 3c,f) is also high for frequency bands with significant variance. Bispectral estimates at P2 (see supporting auxiliary material) suggests a largely linear time series, with little signs of spurious sum-interaction phase coupling. The strong sum-interaction coupling at P3 (supporting auxiliary material) is consistent with a nonlinear shoaling wave, with

a weak coupling between the peak of the spectrum and the infragravity band. Based on the consistency of these results, we will assume that the truncation of the P2 signal is not significant, with P2 probably located slightly above the lowest water level.

Swell propagation direction can be crudely estimated from the phase lag between P3 and P2 (Figure 3b,e, frequency band $0.05\,\mathrm{Hz} \leq f \leq 0.15$ Hz). Allowing for an unknown clock drift of a few seconds, the phase difference in the swell band is not exactly known, whereas the phase difference in the lowest IG band is hardly modified by such a time shift. An equal phase at the two sensors would correspond to waves propagating along-shore, while a cross shore propagation gives a maximum phase shift.

Assuming that 1) P2 and P3 are on the same cross-shore transect; 2) the isobaths are parallel to the shoreline; 3) all modes are progressive waves; and 4) the angle of propagation α is approximately constant between P3 and P2 – one obtains

$$\cos \alpha = \frac{\Theta}{\Delta \theta}; \quad \Delta \theta = \int_{P3}^{P2} k\,dx, \quad (1)$$

where x is the cross-shore axis, $k(f,x)$ is the local wave number, and $\Theta(f)$ is the cross-spectral phase. This yields a swell propagation angle of $\alpha \simeq 66°$, consistent with the large scale propagation direction (Figure 1a). In reality, the angle varies with the position due to refraction, giving a larger contribution to the phase lag, so that this angle is an upper bound of the offshore propagation angle. On mild-sloping plane beach this almost (other conditions have to be met) guarantees the generation of trapped waves.

However, equation 1 cannot be applied to IG band (frequency band $0.05\,\mathrm{Hz} \leq f \leq 0.15$ Hz), where the cross-spectral phase increases (approaching π radians, Figure3b,e), and the integral $\Delta \theta$ decreases, causing the right-hand side of equation 1 to become larger than 1. This suggests that the IG band is a mixture of progressive and standing waves, with the standing waves having a node between P2 and P3 (likely near P3). It is difficult to estimate for the existing data both the propagation angle for the progressive component, and the progressive content of a frequency band. Assuming that the progressive component propagates normal to the shore, the observed cross-spectrum X_{Obs} can be approximated as

$$X_{Obs} = \left(\sqrt{S_2 S_3}\right)_P \cos \Delta\theta \pm \left(\sqrt{S_2 S_3}\right)_S + i\left(\sqrt{S_2 S_3}\right)_P \sin \Delta\theta \quad (2)$$

where $S_{2,3}(f)$ are variance densities at P2 and P3. From equation 2 it is straightforward to estimate the progressive content of a frequency band f as

$$R = \frac{\left(\sqrt{S_2 S_3}\right)_P}{\left(\sqrt{S_2 S_3}\right)_S + \left(\sqrt{S_2 S_3}\right)_P}. \quad (3)$$

Note that $R(f)$ given by equation 3 provides the upper bound of the progressive content, because the propagation direction of the progressive component is not accounted for.

The distribution of $R(f)$ is plotted in Figure3e (circles). The character of the IG band shifts from essentially progressive at high IG frequencies ($R \simeq 0.7$ for $0.015\,\mathrm{Hz} \leq f \leq 0.02$ Hz), to essentially standing at low IG frequencies ($R \simeq 0.3$ for $0.001\,\mathrm{Hz} \leq f \leq 0.003$ Hz). Remarkably, this change in character corresponds to two coherency peaks (Figure 3d-f), that allow one to identify two distinct sub-bands: one centered around the 80-s spectral band, the other centered around 300-s band.

The 80-s band dominates the infragravity band at P3. It has a progressive character, (Figure 3e), and has similar spectral density shapes at P3 and P2 (Figures 3d and 4d). A simple linear shoaling calculation based on the ratio of band variance (P2 to P3) (approximately 4.9) yields for the depth of P2 a hypothetical depth of approximately 0.3 m, consistent with the suggestion that P2 could emerge from the water in wave troughs.

The structure of the 300-s band is essentially standing. Although the P2 and P3 signals are coherent, the spectral shapes are different

and the band variance ratio from (P2 to P3) of approximately 36, a 6-fold increase in amplitude. This cannot be explained by shoaling. Its periodicity, large variance at P2, and its contribution to the time series recorded at P2 (Figure 4a-c) suggests that the 300-s band is responsible for the large, slow oscillations of the water level (see Figure 2c).

Nonlinear shoaling simulations reproduce well the shape of the spectra estimated at P3 and P4 (not shown). Because the model cannot handle wet/dry conditions, the model cannot be used to directly address run-up physics, for example, the role of swash interactions. However, the model can be used to check the degree of consistency between observations and direct IGW generation through nonlinear shoaling. For the sake of comparison, the P2 spectrum is compared with the model output in 0.5 m of water (Figure 4e; consistent with the simple linear shoaling calculations discussed above). Despite the restrictive assumptions of the model, the results suggest that the 80-s band observed at P3 and P2 is consistent with a nonlinearly generated infragravity wave field. Note that there is no hint in the numerical simulations of an emerging 300-s wave as observed at P2. This failure can be easily dismissed as a fault of the nonlinear shoaling model (e.g., lack of directionality). However, in light of the good agreement between the model and P3-P4 observations, we interpret this failure as a suggestion that the 300-s wave is not *directly* generated by the nonlinear shoaling process.

The standing character of the wave and the position of the first node, surprisingly close to the shoreline, as well as its apparent disconnection from the general shoaling process, are consistent with the hypothesis that the 300-s wave is a standing wave trapped on the island platform. Remarkably, Ardhuin et al. [2011] showed that over the seven months of measurements, the 10-minute maximum water levels are highly correlated ($r^2 = 0.9$) to wave parameters modeled in 20~m depth between Banneg and Ouessant. The high correlation between observed high water levels and modeled wave parameters explains 90% of the variance, essentially excluding the possibility that the large water levels were generated by atmospheric pressure perturbations not strongly correlated with waves (rissaga-type oscillations, e.g., Monserrat and Thorpe, 1992; Vennel, 2010).

In summary, statistics indicate a strong correlation between the 300-s wave and the presence of swell, but its generation is not explained by straightforward nonlinear shoaling. We hypothesize that the 300-s wave is generated, not directly by nonlinear interactions with the shoaling swell, but by nonlinear interactions *within* the IG wave family. The energy cascade within the trapped IGW differs significantly from the "simple", "leaky" (that is, not trapped) swell-IGW nonlinear mechanism implemented by the model. Nonlinear interactions between trapped IG waves typically contain resonant triads, which are an efficient and highly-selective nonlinear coupling mechanism. The nature of the trapped IGW interactions, however, an essentially a boundary-value problem, can be only understood and modeled using island-scale, spatially distributed observations and modeling.

References

Agnon Y., A. Sheremet, J. Gonsalves, M. Stiassnie (1993): A unidirectional model for shoaling gravity wave. Coastal Eng., 20, 29-58.

Figure 4. Contribution (band-pass Fourier filter) of the infragravity sub-band to the time series recorded at P2 (compare with Figure 2a). a) Entire infragravity signal ($f \leq 0.05$ Hz). b) 300-s band component; c) 80-s component; d) The infragravity band of the variance spectrum with the two sub-bands (black circles: estimates from measurements; continuous line: P2 spectrum; dashed line P3 spectrum; red: 300-s band; blue: 80-s band). Compare with Figure 3d-f. e) Comparison of numerical simulations and observations of spectral density of variance: Model (black) in 0.5 m water depth 1-m water depth; Observations at P2 (red circles).

Agnon,Y. and A. Sheremet (1997). Stochastic nonlinear shoaling of directional spectra. Journal of Fluid Mechanics 345. p. 79-99.

Ardhuin, F., A. Roland, F. Dumas, A.-C. Bennis, A. Sentchev, P. Forget, J. Wolf, F. Girard, P. Osuna, and M. Benoit (2012). Numerical Wave Modeling in Conditions with Strong Currents: Dissipation, Refraction, and Relative Wind, J. Phys. Oceang. 42/12, 2101-2120. DOI: 10.1175/JPO-D-11-0220.1.

Ardhuin, F., L. Pineau-Guillou, B. Fichaut, and S. Suanez (2011). Extreme set-up and run-up on steep cliffs (Banneg Island, France), 12th International Workshop on Wave Hindcasting and Forecasting, and 3rd Coastal Hazard Symposium Kohala Coast, Hawai'i, HI, 2011.

Aucan J., and F. Ardhuin (2013), Infragravity waves in the deep ocean: An upward revision, Geophys. Res. Lett., 40, 3435–3439, doi:10.1002/grl.50321.

Bryan, K. R., and G. Coco (2010), Observations of nonlinear runup patterns on plane and rhythmic beach morphology, J. Geophys. Res., 115, C09017, doi:10.1029/2009JC005721.

Cariolet J.M., S. Costa, R. Caspar, F. Ardhuin, R. Magne, and G. Goasguen (2010). Atmospheric and marine aspects of the 10th of March 2008 storm in Atlantic and in the Channel", Norois, 215.

Coco, G., Werner, B.T., Burnet, T., Elgar, S. (2004). The role of tides in beach cusp development. Journal of Geophysical Research 109,

CO4011. doi:10.1029/ 2003JC002154.

Elgar, S., Herbers, T. H. C., Chandran, V., & Guza, R. T (1995). Higher-order spectral analysis of nonlinear ocean surface gravity waves, J. Geophys. Res. 100(C3), 4977-4983, doi:10.1029/94JC02900.

Fichaut, B., and S. Suanez (2008). Les blocs cyclopéens de l'île de Banneg (archipel de Molène, Finistère): accumulations supratidales de forte énergie. Geomorphologie: relief, processus, environnement 1, 15-32.

Fichaut, B., and S. Suanez (2011). Quarrying, transport, and deposition of cliff-top storm deposits during extreme events: Banneg Island, Brittany, Mar. Geo., 283(1-4), 36-55. doi:10.1016/j.margeo.2010.11.003

Fritz, H. M., J. C. Borrero, C. E. Synolakis, and J. Yoo (2006). 2004 Indian Ocean tsunami flow velocity measurements from survivor videos, Geophys. Res. Lett., 33, L24605, doi:10.1029/2006GL026784.

Guza, R.T. and E.B. Thornton (1982), Swash Oscillations on a Natural Beach, J. Geophys. Res. 87/C1, 483-491.

Guza R.T. and F. Feddersen (2012). Effect of wave frequency and directional spread on shoreline runup, Geophys. Res. Lett., 39, L11607, doi:10.1029/2012GL051959.

Guza, R.T., and E. B. Thornton (1985). Observations of surf beat. Journal of Geophysical Research, 90, 3161-3172.

Hansom, J.D., N.D.P. Barltrop, and A.M. Hall (2008). Modelling the processes of cliff-top erosion and deposition under extreme storm waves, Mar. Geo. 253 (1-2), 36-50, doi:10.1016/j.margeo.2008.02.015.

Huisman, C.E., K.R. Bryan, G. Coco, and B.G. Ruessink (2011). The use of video imagery to analyse groundwater and shoreline dynamics on a dissipative beach, Cont. Shelf Res. 31, 1728–1738.

Kaihatu, J. M., and J. T. Kirby (1995). Nonlinear transformation of waves in finite water depth. Phys. Fluids, 7, 1903-1914.

Monserrat, S. and A.J. Thorpe (1992). Gravity-wave observations using an array of microbarographs in the Alearic Islands. Q. J. R. Meteorol. Soc., 118, 259-282.

Nwogu, O. and Z. Demirbilek (2010). Infragravity Wave Motions and Runup over Shallow Fringing Reefs, ASCE J. Waterw., Port, Coastal, Ocean Eng. doi: 10.1061/(ASCE)WW.1943-5460.0000050)

Raubenheimer, B., R.T. Guza, and S. Elgar (2001). Field observations of wave-driven setdown and setup. J. Geophy. Res., 106(C3):4629-4638.

Senechal, N., G. Coco, K. R. Bryan, and R. A. Holman (2011), Wave runup during extreme storm conditions, J. Geophys. Res., 116, C07032, doi:10.1029/2010JC006819.

Sheremet, A., R. T. Guza, S. Elgar, and T. H. C. Herbers (2002). Observations of nearshore infragravity waves: Seaward and shoreward propagating components, J. Geophys. Res. 107(C8), 3095, doi: 10.1029/2001JC000970.

Sheremet, A., J.M. Kaihatu, S.-F. Su, E.R. Smith, and J.M. Smith (2011). Modeling of nonlinear wave propagation over fringing reefs, Coastal Eng. 58, 1125–1137, 2011.

Sheremet, A., U. Gravois, and M. Tian (2012). Boat-Wake Statistics at Jensen Beach, Florida , J. Waterw. Port, Coastal, and Ocean Eng. in print.

Suanez, S., Fichaut, B., Magne, R. (2009). Cliff-top storm deposits on Banneg Island, Brittany, France: effects of giant waves in the Eastern Atlantic Ocean. Sedimentary Geology 220 (1-2), 12-28.

Thornton, E.B., and R.T. Guza (1983): Transformation of wave height distribution. J. Geophys. Res. 88, 5925-5938.

Vennell, R. (2010). Resonance and trapping of topographic transient ocean waves generated by a moving atmospheric disturbance. J. Fluid Mech., 650, 427-442.

Vetter, O., J. M. Becker, M. A. Merrifield, A.-C. Pequignet, J. Aucan, S. J. Boc, and C. E. Pollock (2010), Wave setup over a Pacific Island fringing reef, J. Geophys. Res. , 115 , C12066, doi:10.1029/2010JC006455

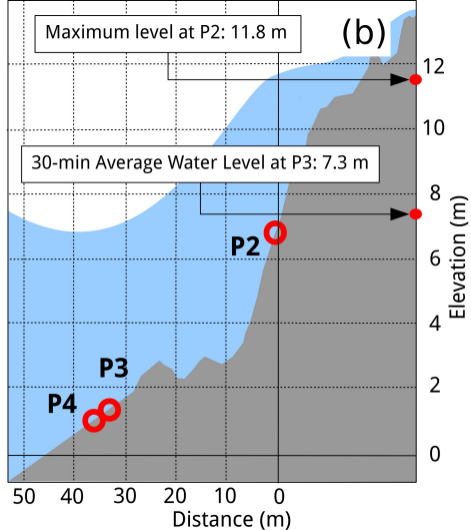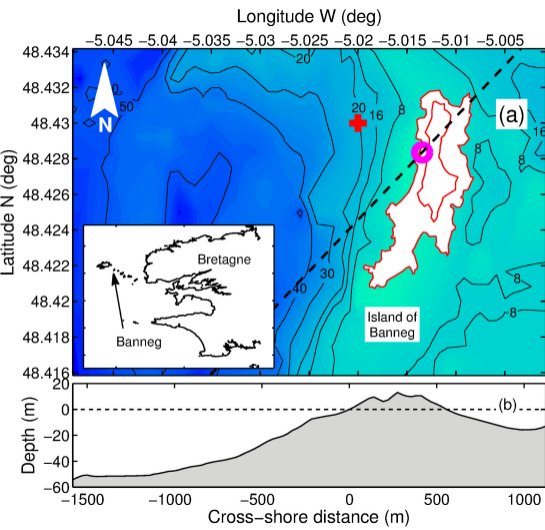Whitham, G. B. (1979). Lectures on Wave Propagation. Tata Institute of Fundamental Research, Bombay.

A. Sheremet, Civil and Coastal Engineering, 365 Weil Hall, University of Florida, Gainesville, FL32611, USA.

T. Staples, Civil and Coastal Engineering, 365 Weil Hall, University of Florida, Gainesville, FL32611, USA. (tmartz@ufl.edu)

F. Ardhuin, IFREMER, Laboratoire d'Océanographie Spatiale, Plouzané, France

S. Suanez, LEGT-Géomer-Brest, IUEM, Plouzané, France.

B. Fichaut, LEGT-Géomer-Brest, IUEM, Plouzané, France.

Longitude W (deg)

Latitude N (deg)

Depth (m)

Cross-shore distance (m)

Bretagne

Banneg

Island of Banneg

Maximum level at P2: 11.8 m

30-min Average Water Level at P3: 7.3 m

Elevation (m)

Distance (m)

P2

P3

P4